Isoscalar transition rates via ^{40}Ca, ^{208}Pb(α,α') at 79 MeV†

L. L. Rutledge, Jr.* and J. C. Hiebert
Cyclotron Institute and Physics Department, Texas A&M University, College Station, Texas 77843
(Received 29 September 1975)

The inelastic scattering of α particles from ^{40}Ca and ^{208}Pb has been studied at a bombarding energy of 79.1 MeV. Isoscalar transition rates have been extracted for the 2^+ level at 3.90 MeV, the 3^- levels at 3.73, 6.29, and 6.58 MeV, and the 5^- level at 4.48 MeV in ^{40}Ca. These have been compared with previous results, and a slight energy dependence is evident. In the case of ^{208}Pb, the isoscalar transition rates have been extracted for the 2^+ level at 4.09 MeV, the 3^- level at 2.62, and the 5^- levels at 3.22 and 3.73 MeV. The analysis of the Coulomb and nuclear interference for the 2^+ level at 4.09 MeV indicates that $\beta_{\text{Coulomb}} = 1.2\beta_{\text{nuclear}}$. A folding model analysis has been made for the 3.73-MeV (3^-) and 3.90-MeV (2^+) levels in ^{40}Ca and the 2.62-MeV (3^-) and 4.09-MeV (2^+) levels in ^{208}Pb. This analysis, using an effective α particle, bound nucleon interaction determined from 79-MeV elastic α-scattering data, is compared with a standard deformed optical potential analysis. Agreement between the two analyses is best for the 2^+ state in ^{208}Pb and worst for the 3^- state in ^{40}Ca. The explicit inclusion of exchange effects tends to reduce the discrepancy between the two reaction models.

[NUCLEAR REACTIONS ^{40}Ca, ^{208}Pb(α,α'), $E = 79.1$ MeV; enriched targets; measured $\sigma(\theta)$; $\theta = 3°$–$40°$; isoscalar transition rates; DWBA analysis, deformed optical potential and folding model form factors.]

I. INTRODUCTION

The inelastic scattering of α particles has provided much nuclear structure information. Because the α particle is strongly absorbed, the dominant mechanism is diffraction scattering. The result is that for even-even nuclei the shape of the inelastic scattering angular distribution depends only on the J^π of the final state. The Blair-Austern diffraction model[1] and the distorted wave Born approximation (DWBA), using deformed optical potentials[2] based on the collective model, both predict accurate shapes for the (α,α') angular distributions. Thus analysis of the shapes of (α,α') angular distributions in terms of these models has yielded reliable J^π assignments to the low-lying states of even-even nuclei. The magnitude of the differential cross section, as interpreted by these models, is related to the average magnitude of some collective coordinate and is not related in any rigorous fashion to the microscopic structure of levels involved. Although the angular distributions show less structure in general, similar analyses of (p,p') and (^{3}He, ^{3}He′) data have been successful.

It has been argued by Bernstein[3] that, in the case of (α,α') angular distributions, the magnitude of the differential cross section can be related to the microscopic structure of the initial and final states. The effective transition operator for (α,α') reactions can to a good approximation be replaced by the isoscalar multipole operator:

$$O(\text{IS}) = \frac{Z}{A} \sum_{\text{nucleons}} r^L Y_L^M(\Omega).$$

Using the usual DWBA analysis with collective model form factors, the extracted deformation length $\beta_L R$ can be used to compute, in a model-independent fashion, the isoscalar transition rate G_L. This quantity is related directly to the matrix element of O(IS) between the initial and final state. The procedure for extracting G_L has been explained in detail in Ref. 3 and will not be repeated here.

In order to establish the extent to which the magnitude of the (α,α') angular distribution can provide nuclear structure information, the above analysis must be applied to many different target nuclei at several bombarding energies. It is also useful to compare rates extracted from (α,α') data to those extracted from (p,p') and (^{3}He, ^{3}He′) data. Additional insight may be provided by analysis in terms of the folding model[4] in which collective model form factors are derived from a deformed matter density. In light of these considerations, the inelastic scattering of α particles from ^{40}Ca and ^{208}Pb was studied at a bombarding energy of 79.1 MeV. The strongly excited 2^+, 3^-, and 5^- levels of the doubly-magic ^{40}Ca and ^{208}Pb were chosen for analysis in terms of a collective model of nuclear motion. Two derivations of collective model form factors for inelastic scattering were used.

First, the usual deformed optical potential form factors[2] are used to analyze the (α,α') angular distributions. In this model, which was also used by Bernstein,[3] the elastic scattering data are described in terms of a Woods-Saxon optical potential:

$$U(r_\alpha) = -(V+iW)\{1+\exp[(r_\alpha - R_0)/a]\}^{-1}, \quad (1)$$

where

$$R_0 = r_0 A^{1/3}.$$

The form factor for inelastic scattering, derived from the deformed components of the optical potential, is given by

$$\langle J_f = l \,||\, V_l \,||\, J_i = 0\rangle = -i^l (2l+1)^{-1/2} \beta_l R_0 \frac{d}{dr_\alpha} U(r_\alpha). \quad (2)$$

The second version of the collective model form factor is that suggested by Rawitscher and Spicuzza.[4] In this model the elastic scattering is described in terms of a microscopic optical potential. The optical potential is obtained by folding an effective α-particle bound-nucleon interaction into the matter distribution of the target nucleus:

$$U(r_\alpha) = (\lambda_R + i\lambda_I) \int \rho(r) V_{\text{eff}}(|\vec{r} - \vec{r}_\alpha|) d\vec{r}. \quad (3)$$

The effective interaction V_{eff} used in the present work consists of a direct term and a one particle exchange term. The direct term is that derived by Bernstein[3] from the empirical α-particle size and nucleon-nucleon interaction. A Gaussian form with a depth $V_0 = 37$ MeV and a range $\beta = 2$ fm was obtained. The one particle exchange term, or exchange pseudopotential, was derived in a fashion similar to that of Schaeffer,[5] except that, for the sake of consistency, the α-particle matter distribution and nucleon-nucleon interaction employed by Bernstein[3] was used. This results in a Gaussian shape with a range $\beta = 1.31$ fm and a depth

$$V_0 = (129)\exp(-0.58k^2) \text{ MeV},$$

where k is $\frac{1}{4}$ the incident α-particle momentum in fm^{-1}. The parameters λ_R and λ_I are adjusted to fit the 79-MeV elastic α scattering. In this work, the importance of explicitly including exchange is probed by performing the analyses both with and without the exchange pseudopotential. The form factor for inelastic scattering, derived from the deformed components of the matter distribution which are related to those of the optical potential via Eq. (3), is given by

$$\langle J_f = l \,||\, V_l \,||\, J_i = 0\rangle = -i^l (2l+1)^{-1/2} \beta_l^m R_0^m \times \int \frac{d\rho(r)}{dr} V_l(r_\alpha, r) r^2 dr, \quad (4)$$

where $V_l(r_\alpha, r)$ is a coefficient in the expansion of $(\lambda_R + i\lambda_I)\, V_{\text{eff}}$ in spherical harmonics.

It has been suggested[6] that this model must be used with caution. One reason for this is that exchange terms have been ignored. Also, no attention has been given to the self-consistency of the density and potential vibrations. It has also been shown that the transition density is sensitive to the form of deformation assumed. The effect will, in general, depend on the multipolarity of the transition. Therefore a direct comparison of this model with the deformed potential model can be misleading.

On the other hand, the folding model does have appealing simplicity. This model also has the advantage that the effective α-particle, bound-nucleon interaction has been distinguished from the transition density. This allows further development of the model not possible with the deformed potential model. For instance, the importance of exchange can be estimated by using the pseudopotential of Schaeffer.[5] In the case of α scattering, if one can assume that the interaction is known, the transition density could be experimentally extracted in the surface region.[7] The success of the microscopic analysis in extracting information about the matter density from elastic α-particle scattering data encourages such a procedure. Therefore, an analysis of the inelastic data in terms of both the deformed potential and folding models is of interest.

II. ANALYSIS OF ELASTIC SCATTERING DATA

It has been suggested[8] that the optical potential and the form factor for inelastic scattering must be generated in a consistent fashion. Thus, in the present work the optical potential used to generate the distorted waves is also used to generate the form factor in every case. The different analyses of the inelastic scattering data each necessitated a separate analysis of the elastic scattering data.

Table I shows the Woods-Saxon potential parameters obtained from an analysis of previously measured elastic scattering data.[9-11] It is well known that there is considerable ambiguity in the optical model parameters for elastic scattering of α particles. This is especially severe if the data are restricted to the diffraction region. However, we have found that the quantity $\beta_L R_0$ extracted from an analysis of the inelastic scattering data is independent of the optical potential so long as the

TABLE I. Optical potential parameters.

Potential		V (MeV)	W (MeV)	r_0 (fm)	a (fm)
^{40}Ca	Shallow	50.0	25.9	1.58	0.66
^{40}Ca	Deep	200.0	79.8	1.30	0.66
^{208}Pb	Shallow	50.0	33.6	1.45	0.66
^{208}Pb	Deep	171.5	105.6	1.30	0.67

optical potential describes the elastic scattering.

In the case of ^{40}Ca the procedure of Bernstein and Seidler[12,13] is used in the analysis in terms of the microscopic optical potential. The matter distribution $\rho(\vec{r})$ is taken to be twice the charge distribution[14] with the proton charge form factor unfolded. An exponential shape with an rms radius of 0.8 fm was used for the proton form factor.[15] The strength parameters λ_R and λ_I were adjusted to give the best fit to the ^{40}Ca elastic scattering in the diffraction region, and the result is $\lambda_R = 1.018$ and $\lambda_I = 0.473$. If the exchange pseudopotential is included we obtain $\lambda_R = 0.847$ and $\lambda_I = 0.377$.

For ^{208}Pb, the matter distribution is parametrized as a Fermi density,

$$\rho(r) = \rho_0\{1 + \exp[(r - c)/a]\}^{-1} .$$

Taking λ_R and λ_I from the ^{40}Ca results and varying c and a, as suggested by Bernstein and Seidler,[12,13] it was not possible to find a satisfactory fit to the ^{208}Pb elastic scattering data. Figure 1 shows the angular distribution for the elastic scattering of 79.1-MeV α particles from ^{208}Pb. The dashed curve shows the optical model calculation when the Bernstein-Seidler prescription is used. Including the exchange pseudopotential and using the appropriate λ_R and λ_I does not change the quality of the fit. The solid curve shows the optical model calculation using the Woods-Saxon potentials of Table I. The relative amount of absorption W/V for the "shallow" potential is 0.67 and for the "deep" is 0.62. This is to be compared with $\lambda_I/\lambda_R = 0.46$, or 0.44 if the exchange pseudopotential is utilized, from the analysis of ^{40}Ca(α,α).

Allowing λ_I to vary along with the parameters of the matter distribution results in an optical model fit of the same quality as the solid curve in Fig. 1. Although the Bernstein-Seidler prescription which works well[11-13] for ^{16}O, ^{28}Si, ^{40}Ca, ^{48}Ca, and ^{90}Zr fails to give an acceptable fit for ^{208}Pb(α,α) at 79.1 MeV, it is gratifying that a good fit can be achieved by allowing only λ_I to vary. For the best fit, the relative amount of absorption is found to be $\lambda_I/\lambda_R = 0.65$ and the rms matter radius is $\langle r^2\rangle^{1/2} = 5.57$ fm. Including the exchange pseudopotential results in no change in either the relative absorption or the quality of the fit to the elastic scattering data. The rms matter radius in this case is $\langle r^2\rangle^{1/2} = 5.53$ fm. The results for the rms matter radius are compared to the results of other experiments[13,16-21] in Table II. The agreement is in general good, especially among the (α,α) results.

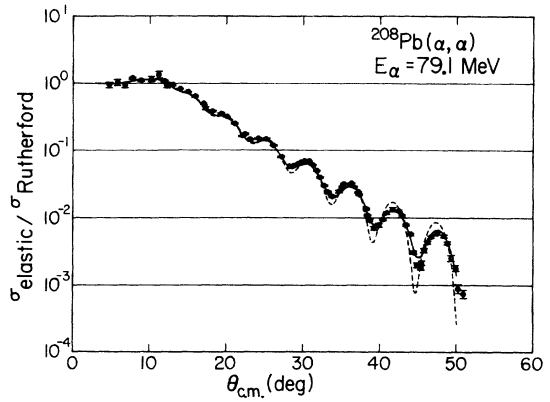

FIG. 1. Angular distribution of α particles elastically scattered from ^{208}Pb at a bombarding energy of 79.1 MeV. The dashed curve shows the best fit obtained from an analysis using a microscopic optical potential and the procedure of Bernstein and Seidler. The solid curve shows the best fit obtained using a Woods-Saxon optical potential.

III. EXPERIMENTAL PROCEDURE

α particles were accelerated to an energy of 79.1 MeV by the Texas A&M variable energy cyclotron. The extracted beam was passed through a 159.5° analyzing magnet and focused on target with the aid of several quadrupole doublets. A set of three slits was used to define a 3-mm-wide beam spot on target. The targets consisted of self-supporting metal foils of ^{40}Ca and ^{208}Pb having isotopic purities of 97 and 99%, respectively. Several uniform foils of each element varying from 0.5 to 1.5 mg/cm^2 in thickness were used. A Faraday cup positioned behind the target and inside the 41-cm scattering chamber was used to stop the unscattered beam. This Faraday cup provided an approximate monitor of the amount of beam on target. The scattered beam was analyzed by an Enge split-pole spectrograph and was detected with a 1

TABLE II. ^{208}Pb rms radii.

Technique	$\langle r^2\rangle^{1/2}$ (fm)
(α,α) $E_\alpha = 79.1$ MeV [a]	
Bernstein's prescription	5.70 ± 0.10
Direct term only	5.57 ± 0.10
Direct + exchange	5.53 ± 0.10
(α,α) $E_\alpha = 104$ MeV [b]	5.59 ± 0.06
(α,α) $E_\alpha = 140$ MeV [b]	5.69 ± 0.10
(α,α) $E_\alpha = 166$ MeV [b,c]	5.65 ± 0.10
Coulomb energy difference [b,d]	5.54
(p,p) $E_p = 30$ MeV [b,e]	5.66 ± 0.20
(p,p) $P_p = 19.3$ GeV/c [b,f]	5.49
Coherent (γ,π^0) [b,g]	5.78 ± 0.30
Coherent (γ,ρ) [b,h]	5.66 ± 0.15

[a] Present experiment.
[b] Reference 13.
[c] Reference 16.
[d] Reference 17.
[e] Reference 18.
[f] Reference 19.
[g] Reference 20.
[h] Reference 21.

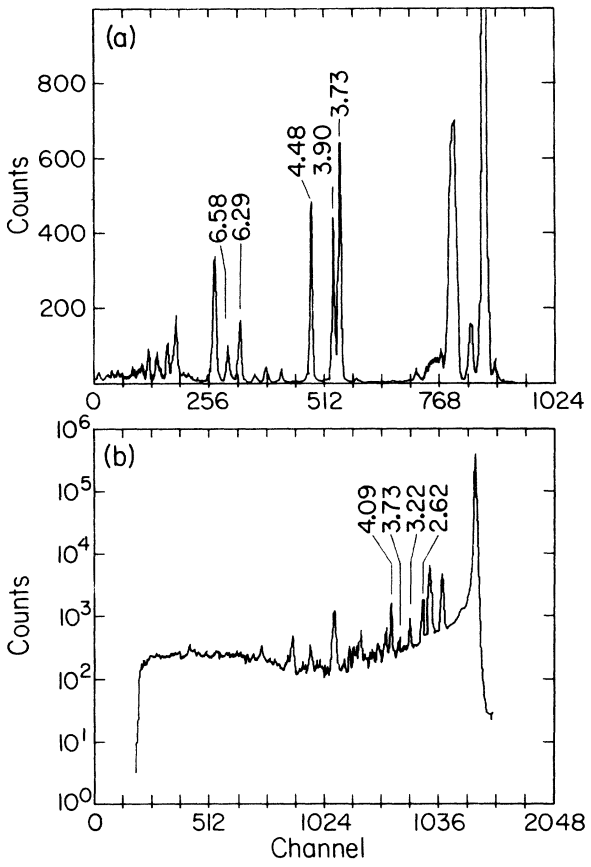

FIG. 2. Position spectrum of α particles inelastically scattered from (a) ^{40}Ca and (b) ^{208}Pb at a bombarding energy of 79.1 MeV.

×30-cm position-sensitive single-wire charge-division proportional counter. A plastic scintillator placed behind the counter gave a measure of the total energy of the detected particle. The scintillator signal was used to gate signals from the proportional counter, thereby eliminating the unwanted x-ray and γ-ray background. The low-energy continuum of deuterons from the (α, d) reaction was removed from the α-particle spectrum by placing a digital baseline on the sum of the signals from the ends of the proportional counter.

A position spectrum of α particles inelastically scattered from ^{40}Ca is shown in Fig. 2(a). Peaks corresponding to the excitation of the well-known 3^- levels at 3.73, 6.29, and 6.58 MeV, the 2^+ level at 3.90 MeV, and the 5^- level at 4.48 MeV are indicated. An angular acceptance of 0.5° was used to obtain spectra at laboratory scattering angles between 3.0° and 15.0°. For angles between 15.0° and 36.0°, the angular acceptance was 2.0°. The energy resolution was about 70 keV [full width at half maximum (FWHM)]. This corresponds to a position resolution of about 1.1 mm. Figure 2(b) shows a typical spectrum of inelastically scattered α particles from ^{208}Pb at a bombarding energy of 79.1 MeV. In the case of ^{208}Pb spectra were obtained at laboratory scattering angles between 6.0° and 40.0°. An angular acceptance of 0.5° was used in order that any interference between Coulomb and nuclear excitation would not be obscured. The resolution was about 85 keV (FWHM). This corresponds to a position resolution of about 1.35 mm. Peaks corresponding to the excitation of the well-known 3^- level at 2.62 MeV, the 5^- levels at 3.22 and 3.73 MeV, and the 2^+ level at 4.09 MeV are indicated in Fig. 2(b).

IV. ^{40}Ca ANGULAR DISTRIBUTIONS

The differential cross sections for the various excited states of ^{40}Ca were calculated by comparing the peak yields to the yield of the elastic peak. The differential cross section for elastic scattering was obtained by interpolating the previously measured values.[9] The correction for the change in center-of-mass solid angle due to a change in excitation energy was, of course, included. The statistical uncertainty and the estimated uncertainty in the interpolation of the elastic scattering cross section are included in the error bars. An additional 5% uncertainty in the absolute normalization due to the uncertainty in the absolute normalization of the elastic scattering data, was not included.

The angular distributions for the inelastic scattering of 79.1-MeV α particles from ^{40}Ca are presented in Fig. 3 for the well-known 2^+, 3^-, and 5^- levels. The solid curves are the DWBA predictions obtained using the deformed optical potential form factors. There is excellent over-all agreement in all cases. However, for the higher-lying 3^- levels at 6.29 and 6.58 MeV, the model predictions do show slight deviations from the data beyond the second diffraction maxima. The minima of the oscillations of the data are slightly shifted to smaller angles relative to the model predictions. These two levels have much weaker isoscalar transition rates relative to the 3^- level at 3.73 MeV whose angular distribution has oscillations in phase with the model predictions. This may indicate the beginnings of a breakdown of the model for these less collective levels. The angular distribution for both the 2^+ level at 3.90 MeV and the 5^- level at 4.48 MeV also have the phase of their oscillations well described by the DWBA.

The results for the inelastic scattering of α particles from ^{40}Ca are summarized in Table III. The extracted isoscalar transition rates are compared to those extracted at 30-MeV (Ref. 22) and 50-MeV (Ref. 23) bombarding energies. The reduced tran-

sition rates from a recent inelastic proton study[24] are also included. The extracted rates at 79 MeV include the Coulomb excitation contribution and the smooth falloff of the matter density at the nuclear surface has been taken into account.[3] The uncertainty in the extracted isoscalar transition rates is 15%. This does not include systematic model-dependent errors. It is interesting that the extracted (α,α') transition rates decrease with increasing bombarding energy in a consistent fashion. It has been pointed out[3] that a comparison of (α,α') and (p,p') rates may be valid only for the highly collective excitations. The proton is more penetrating and, in addition, has spin and isospin degrees of freedom. In light of this, it is interesting that the proton results are in better agreement with the higher energy (α,α') results with the exception of the lowest 3^- and 5^- levels. For these two levels, which are highly collective in nature and can be described accurately in terms of one-particle-one-hole configurations,[25] the proton results are in better agreement with the lower energy (α,α') results.

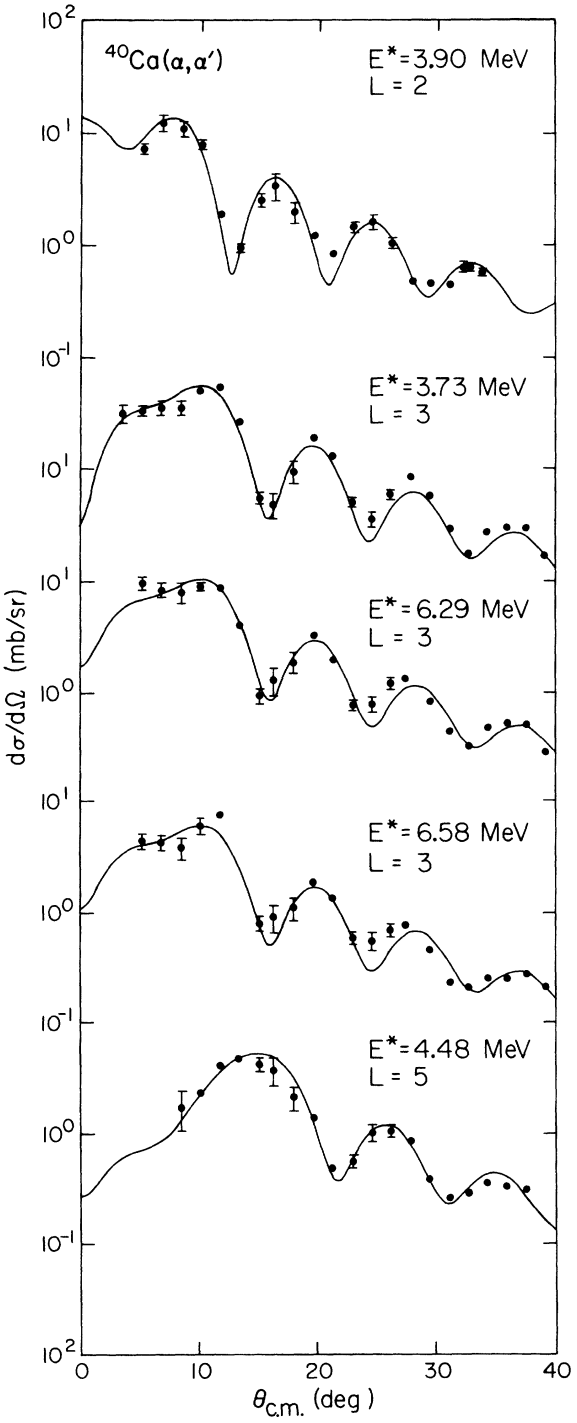

FIG. 3. Angular distributions of 79.1-MeV α particles inelastically scattered from ^{40}Ca. The solid curves are the DWBA predictions using the deformed optical potential form factors.

V. ^{208}Pb ANGULAR DISTRIBUTIONS

The differential cross sections for the excitation levels in ^{208}Pb were determined by normalizing the peak yields to the elastic peak yield in a manner similar to that for the ^{40}Ca data. A uniform 10% uncertainty was assigned to each data point except when the statistical uncertainty was large. The larger uncertainty was used because of the large background due to the elastic peak tail. An additional 5% uncertainty in the absolute normalization has not been included. This uncertainty stems from the uncertainty in the absolute normalization of the elastic scattering angular distribution.

Figure 4(a) shows the angular distribution for the well-known 2^+ level at an excitation energy of 4.09 MeV. The solid curve is the DWBA prediction for $L=2$ using the deformed optical potential form factors. For partial waves up to $l=100$, both the nuclear and Coulomb contributions were included. This calculation is indicated by the dashed curve in Fig. 4(a). The contribution from the nuclear interaction is negligible for higher partial waves. The Coulomb interaction matrix elements are, however, important, and these have been included for partial waves up to $l=200$.[26] Including more than 200 partial waves does not change the predicted angular distribution which is shown as a solid curve. It is found that using more than 100 partial waves improved the agreement between the DWBA prediction and the data at small angles. However, the extracted isoscalar transition rate of 7.0 s.p.u. (single-particle units) was not changed.

Figure 4(b) shows the angular distributions for the excitation of the 3^- level at 2.62 MeV and the 5^- levels at 3.22 and 3.73 MeV. The solid curves are the DWBA predictions using the deformed op-

TABLE III. ^{40}Ca reduced transition rates.

		G_L [a]			
E^*	L	(α,α') [b] 30.1 MeV	(α,α') [c] 50.9 MeV	(α,α') [d] 79.1 MeV	(p,p') [e] 40 MeV
3.73	3	23.6	19.5	15.3	28.7
3.90	2	2.9	2.2	1.8	2.05
4.48	5	17.7	11.3	8.0	20.6
6.29	3	6.6	4.1	3.0	3.1
6.58	3	3.8	2.3	1.8	2.5

[a] In single-particle units.
[b] Reference 22.
[c] Reference 23.
[d] Present experiment.
[e] Reference 24.

tical potential form factors. For these levels only 100 partial waves have been included, but this is not expected to affect the extracted isoscalar transition rates. The agreement between the data and the DWBA curves is excellent.

Previous analyses of inelastic scattering using the deformed optical potential form factor with the DWBA and including Coulomb excitation have generally assumed that $\beta_{\text{Coulomb}} = \beta_{\text{nuclear}}$. Furthermore, the phase of the nuclear excitation form factor is that predicted by the collective model when both the real and imaginary parts of the optical potential are deformed. For energies near the Coulomb barrier, it has been shown[27] that the predicted cross section at large angles depends strongly on the phase of the nuclear excitation form factor when Coulomb excitation is included. To investigate the effect of the phase of the nuclear excitation in the present case, the restriction $\beta_{\text{Coulomb}} = \beta_{\text{nuclear}}$ was relaxed. Figure 5 shows the angular distribution for the 4.09-MeV level with the nuclear and Coulomb interference region expanded. The solid curve shows the DWBA prediction with $\beta_{\text{Coulomb}} = 1.2\beta_{\text{nuclear}}$. The DWBA prediction for the case with $\beta_{\text{Coulomb}} = 0.9\beta_{\text{nuclear}}$ is indicated by the dashed curve. The data show a clear preference for the larger $\beta_{\text{Coulomb}}/\beta_{\text{nuclear}}$ ratio. The β_{Coulomb} value extracted by normalizing the DWBA calculation to the data is insensitive to these small deviations from unity for this ratio; however, the value of β_{nuclear} is changed by the appropriate amount. This indicates that the extracted isoscalar transition rates could be as much as 40% less than the electromagnetic transition rate.

The results of the inelastic scattering of α particles from ^{208}Pb at a bombarding energy of 79.1 MeV are summarized in Table IV. The uncertainty in the extracted rates is $\pm 15\%$. This does not include systematic model-dependent errors. Where possible a comparison to the 42-MeV α-particle scattering[28] has been made. Also included in Table IV are the transition rates extracted from inelastic proton[29,30] and inelastic ^3He (Ref. 31) scattering experiments. Although the agreement between the (α,α') and the 54-MeV (p,p') rates is good, the comparison must be made with care. The 54-MeV (p,p') rates have been normalized to give a transition rate of 32 s.p.u. for the 3^- level at 2.62 MeV. We note that a (p,p') study at 40 MeV (Ref. 32) reports reduced transition rates in agreement with the 54-MeV (p,p') rates. The 25-MeV (p,p') rates as well as the 44-MeV $(^3He,^3He')$ rates are, on the other hand, significantly lower than the (α,α') rates. The extracted transition rates appear to fall into one of two groups. The (α,α') and higher energy (p,p') rates form one group, while the $(^3He,^3He')$ and lower energy (p,p') rates form the second. More data on the (α,α'), $(^3He,^3He')$, and (p,p') reactions at several different bombarding energies are needed to resolve this discrepancy.

At the risk of interjecting more confusion into this situation, we note with interest the following circumstance. Recall that the angular region of interference between nuclear and Coulomb excitation indicates the $\beta_{\text{Coulomb}} = 1.2\beta_{\text{nuclear}}$ for the 2^+ level at 4.09 MeV. Using this relation, we obtain an electromagnetic transition rate of 7 s.p.u. This is to be compared with 8.1 s.p.u. as determined by (e,e') experiments. Furthermore, the isoscalar transition rate is found to be 4.9 s.p.u. which happens to be in agreement with the $(^3He,^3He')$ and lower energy (p,p') rates.

VI. FOLDING MODEL ANALYSIS

The ability of shell model wave functions to predict the inelastic scattering would provide a good test of their validity. It is necessary, however, to isolate the transition density and to understand its relative importance in the calculation of the inelastic scattering. It must be shown that the effective α-particle bound-nucleon interaction is known with sufficient accuracy before unambiguous infor-

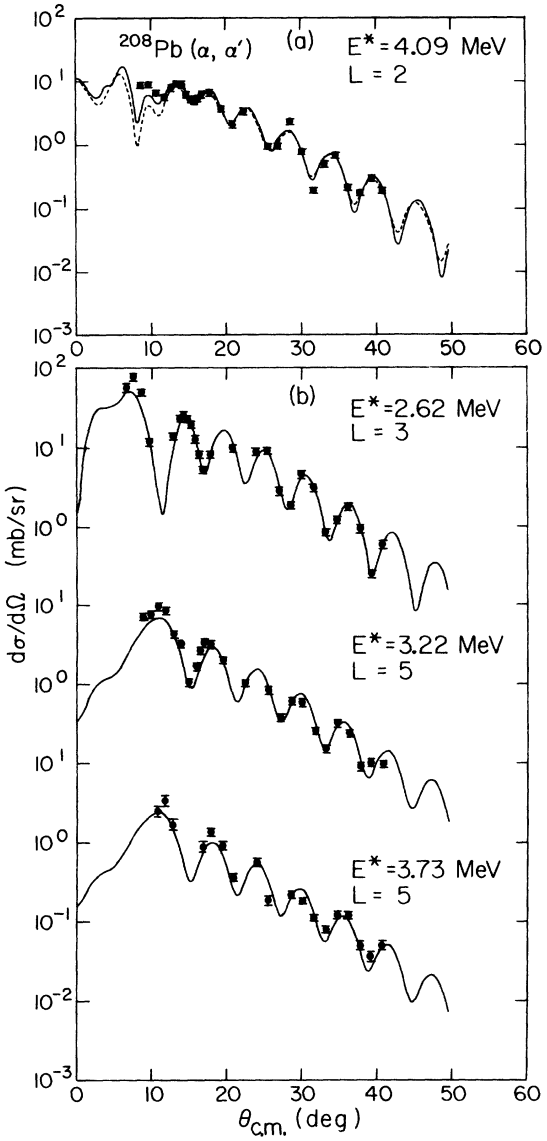

FIG. 4. (a) Angular distribution of 79.1-MeV α particles inelastically scattered from ^{208}Pb exciting the 2^+ level at 4.09 MeV. The solid curve indicates the $L=2$ DWBA prediction using 200 partial waves, while the dashed curve was obtained using 100 partial waves. (b) Angular distributions of α particles inelastically scattered from ^{208}Pb exciting the 3^- level at 2.62 MeV, and the 5^- levels at 3.22 and 3.73 MeV. The solid curves indicate the DWBA predictions using 100 partial waves.

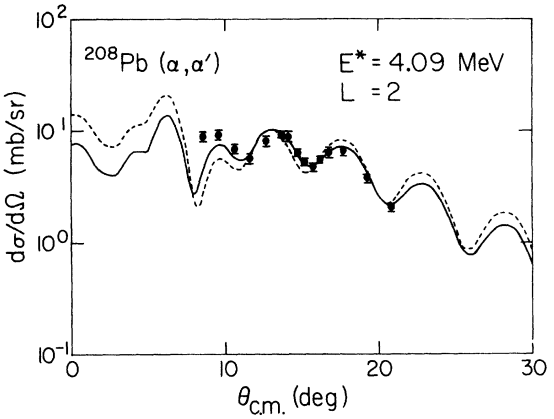

FIG. 5. Nuclear and Coulomb excitation interference region of the angular distribution of α particles inelastically scattered from ^{208}Pb exciting the 2^+ level at 4.09 MeV. The solid curve is the DWBA prediction with $\beta_{\text{Coulomb}} = 1.2\beta_{\text{nuclear}}$, while the dashed curve is the DWBA prediction with $\beta_{\text{Coulomb}} = 0.9\beta_{\text{nuclear}}$.

mation concerning the transition density can be extracted. In particular, it is of interest to know whether or not the effective interaction $(\lambda_R + i\lambda_I)V_{\text{eff}}$ as determined by elastic scattering measurements is sufficiently accurate to explain the inelastic scattering. The form factor for nuclear excitation is obtained by folding the effective interaction into the transition density. Thus information about the transition density can only be extracted insofar as the form factor is determined by the inelastic scattering data.

The 3^- level at 3.73 MeV and the 2^+ level at 3.90 MeV in ^{40}Ca, along with the 3^- level at 2.62 MeV and the 2^+ level at 4.09 MeV in ^{208}Pb, provide good candidates for a folding model analysis of inelastic α-particle scattering. These levels are collective in nature, and hence their angular distributions are well described by the DWBA. It is instructive to first examine the usual deformed optical potential analysis. Figure 6(a) shows the form factors for the "shallow" and "deep" optical potentials. These form factors correspond to the excitation of the 3^- level at 3.73 MeV in ^{40}Ca. It is clear that the inelastic scattering determines the form factor in the surface region beyond ~6 fm. In fact, if the form factor is made to vanish inside 4 fm, the inelastic scattering prediction is not altered. Figure 6(b) shows a somewhat different set of deformed optical potential form factors for the excitation of the 3^- level at 3.73 MeV in ^{40}Ca. These form factors are obtained from the microscopic optical potentials with the direct term only and with the exchange pseudopotential included. The use of these form factors in the DWBA calculations gives inelastic scattering results which are essentially identical to those obtained with the usual form factors derived from Woods-Saxon optical potentials. Of course, it is necessary to use the correct optical model wave functions.

Folding model form factors for the excitation of the 3^- level at 3.73 MeV in ^{40}Ca are shown in Fig. 7.

TABLE IV. ^{208}Pb reduced transition rates.

E^* (MeV)	L	G_L [a] (α,α') [b] 79.1 MeV	(α,α') [c] 42.0 MeV	(p,p') [d] 54.0 MeV	(p,p') [e] 24.6 MeV	(h,h') [f] 43.7 MeV
2.62	3	38.5	35.8	32.0	19.5	19.2
3.22	5	12.1	15.8	9.3	8.1	3.5
3.73	5	4.4		3.8	1.85	
4.09	2	7.0	6.9	8.9	4.6	4.9

[a] In single-particle units.
[b] Present experiment.
[c] Reference 28.
[d] Reference 30.
[e] Reference 29.
[f] Reference 31.

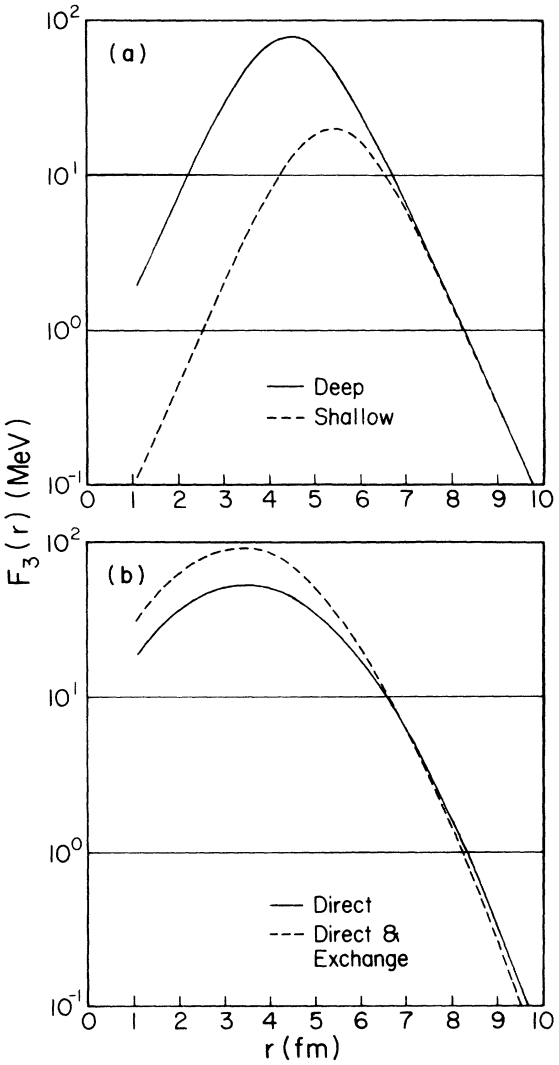

FIG. 6. The real part of the deformed optical potential form factor for the inelastic scattering of 79.1-MeV α particles from ^{40}Ca exciting the 3^- level at 3.73 MeV. The curves in (a) are derived from the Woods-Saxon potentials while those in (b) are derived from the microscopic optical potential of Ref. 11.

The solid curve is the form factor that results if only the direct term is considered explicitly. Higher order effects, including exchange for example, are then taken into account approximately by adjusting λ_R and λ_I to obtain a best fit to the elastic scattering data. The dashed curve is the form factor that results if some exchange effects are included explicitly through the use of the exchange pseudopotential. The shapes of the inelastic scattering angular distributions predicted using

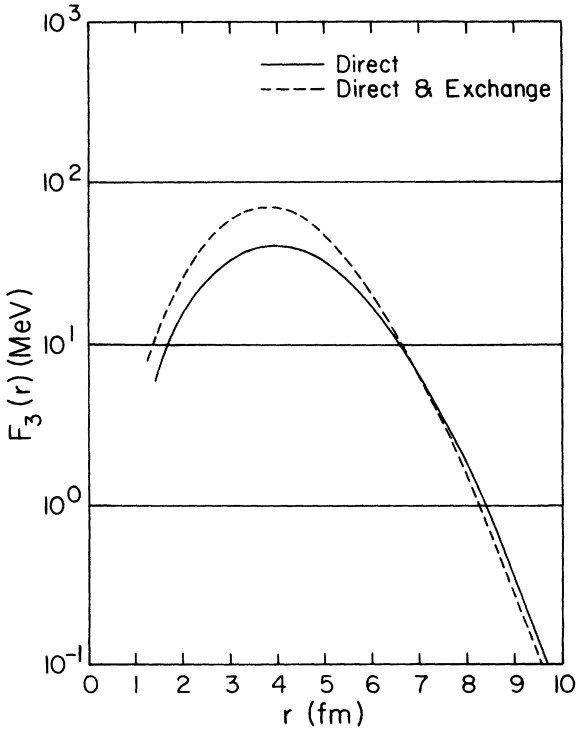

FIG. 7. The real part of the folding model form factor for the inelastic scattering of α particles from ^{40}Ca exciting the 3^- level at 3.73 MeV. The solid curve shows the form factor obtained when only the direct term is considered explicitly, while the dashed curve shows the form factor obtained when use is made of the exchange pseudopotential.

TABLE V. Reduced transition rates.

Nucleus	E^* (MeV)	L	Reaction	Form factor	G_L [a]
^{40}Ca	3.73	3	(α,α') [b]	Deformed optical potential	15.3
				Folding (direct)	34.0
				Folding (direct + exchange)	26.5
			(e,e') [c]		32.0
	3.90	2	(α,α')	Deformed optical potential	1.8
				Folding (direct)	2.7
				Folding (direct + exchange)	2.2
			(e,e')		1.8
^{208}Pb	2.62	3	(α,α')	Deformed optical potential	38.5
				Folding (direct)	45.5
				Folding (direct + exchange)	45.5
			(e,e') [d]		39.5
	4.09	2	(α,α')	Deformed optical potential	7.0
				Folding (direct)	7.2
				Folding (direct + exchange)	7.2
			(e,e')		8.1

[a] In single-particle units.
[b] Present experiment.
[c] Reference 33.
[d] Reference 34.

these form factors are essentially the same as the shapes of the previous deformed optical potential predictions. However, the extracted isoscalar transition rates are highly dependent on the model used.

The shape of any of the previously discussed form factors is derived from the optical potential. Thus the shape of the form factor is determined by the elastic scattering measurements and the model chosen for the calculation. The shape of the predicted angular distribution for the inelastic scattering has been found to be almost independent of the model chosen for the form factor. By normalizing the DWBA predictions to the experimental data, all the various form factors used to describe the excitation of a given level were forced to have approximately the same value in some limited region near the nuclear surface. This point is illustrated in Figs. 6 and 7 for the excitation of the 3^- level at 3.73 MeV in ^{40}Ca.

Similar results were found for the analysis of the 2^+ level at 3.90 MeV in ^{40}Ca, the 3^- level at 2.62 MeV in ^{208}Pb, and the 2^+ level at 4.09 MeV in ^{208}Pb. The isoscalar transition rates extracted using the folding model analysis are given in Table V. Also included are the isoscalar transition rates extracted using the deformed optical potential analysis and the electromagnetic transition rates as determined by (e,e') experiments.[33,34]

Although the shape of the predicted angular distribution is almost model-independent, the extracted isoscalar transition rates are highly model-dependent for the excitation of levels in ^{40}Ca. It appears that the inclusion of exchange somewhat reduces the discrepancy between the folding model and deformed optical potential analyses. This indicates that higher order effects, which are included in the deformed optical potential formulation in a phenomenological way, may have to be accounted for explicitly in the folding model approach. Furthermore, the discrepancy seems to be much less severe for the quadrupole excitation as opposed to the octupole excitation. This indicates that the discrepancy will increase for higher multipoles, since the folding model form factor is known to decrease monotonically with increasing angular momentum transfer. In the quadrupole case the calculations appear to have converged, in some sense, as is indicated by agreement of all the (α,α') rates with the (e,e') rates.

A comparison of the analysis of the ^{208}Pb levels with the analysis of the ^{40}Ca levels should provide information about the A dependence of the extracted isoscalar transition rates. The inclusion of the exchange pseudopotential in the folding model form factor does not change the extracted isoscalar transition rate for either of the levels in ^{208}Pb. This result indicates that the folding model form factor for ^{208}Pb is dominated by the transition density. The details of the effective α-particle bound-nucleon interaction are relatively unimportant in determining the form factor in the region of importance near the nuclear surface. This implies that, in the case of ^{208}Pb, the effective interaction $(\lambda_R+\lambda_I)V_{\text{eff}}$ as determined by elastic scattering is sufficiently accurate for a folding model analysis of the inelastic scattering. Such is not necessarily the case for ^{40}Ca.

In the case of the 3^- level in ^{40}Ca, the absolute normalization of the transition density, which is proportional to the square root of the isoscalar transition rate, depends on whether or not the exchange pseudopotential is included. Without the exchange pseudopotential, all exchange effects are included implicitly by adjusting λ_R and λ_I to fit the elastic data. Because of the ambiguity in the normalization of the transition density, it is concluded that the effective interaction determined by analysis of the elastic scattering data may not necessarily be correct for a folding model analysis of the inelastic scattering to the 3^- level in ^{40}Ca. In particular, exchange effects appear to contribute differently for inelastic scattering than for elastic scattering.

The discrepancy between the folding model and deformed optical potential analyses is less severe in the case of ^{208}Pb. This is because the range of the effective interaction is smaller relative to the nuclear size for ^{208}Pb than for ^{40}Ca. This is important because in the limit of zero range, the folding model and deformed optical potential analyses yield the same form factor.

VII. CONCLUSIONS

The magnitude of the inelastic scattering differential cross section gives limited nuclear structure information at the present time. There is not yet sufficient experimental information to reveal trends, nor is the theoretical machinery for extracting this information highly developed. In the case of the inelastic scattering of α particles from ^{40}Ca, the extracted isoscalar transition rates exhibit a slight energy dependence. This is not observed for the ^{208}Pb(α, α'). The extent of agreement between (α, α') rates with (p, p') and (^{3}He, ^{3}He$'$) rates also exhibits an energy dependence for various levels. No general trends can be recognized, however. The analysis of the Coulomb and nuclear excitation interference indicates that for the lowest 2^+ level in ^{208}Pb, the electromagnetic transition rate can be unambiguously extracted independent of the assumption that $\beta_{\text{Coulomb}} = \beta_{\text{nuclear}}$. However, the isoscalar transition rate may be as much as 40% less than the electromagnetic transition rate.

The use of the folding model analysis indicates that in general exchange effects must be included explicitly. Also the effects of exchange appear to be somewhat different for the elastic scattering than for the inelastic scattering. For these reasons the effective α-particle bound-nucleon interaction obtained from an analysis of elastic scattering data may not necessarily be the correct interaction to use in a folding model analysis of inelastic scattering. The importance of these effects increases with increasing multipolarity of the transition, and with decreasing atomic number. Thus these effects are quite evident for the first 3^- level in ^{40}Ca but negligible for the first 2^+ level in ^{40}Ca and the first 3^- and 2^+ levels in ^{208}Pb.

ACKNOWLEDGMENTS

We would like to thank the Cyclotron Institute staff for their assistance throughout this investigation. In particular we note the help of R. A. Kenefick with the proportional counter and R. L. York with data acquisition. The invaluable contributions of G. M. Lerner to the acquisition and analysis of the elastic scattering data is acknowledged. It is a pleasure to acknowledge many stimulating discussions with A. M. Bernstein.

---

†Work supported in part by the National Science Foundation.

*Present address: Department of Physics, Northwestern University, Evanston, Illinois 60201.

[1]J. S. Blair, in *Lectures in Theoretical Physics*, edited by P. D. Kunz, D. A. Lind, and W. E. Brittin (University of Colorado Press, Boulder, 1965), Vol. VIII C, p. 343.

[2]R. H. Bassel, G. R. Satchler, R. M. Drisko, and E. Rost, Phys. Rev. 128, 2693 (1962).

[3]A. M. Bernstein, in *Advances in Nuclear Physics*, edited by M. Baranger and E. Vogt (Plenum, New York, 1969), Vol. 3.

[4]G. H. Rawitscher and S. A. Spicuzza, Phys. Lett. 37B, 221 (1971).

[5]Richard Schaeffer, Nucl. Phys. A158, 321 (1970).

[6]G. R. Satchler, Phys. Lett. 39B, 495 (1972).

[7]A. M. Bernstein (private communication).

[8]D. F. Jackson, Phys. Lett. 14, 118 (1965).

[9]G. M. Lerner, J. C. Hiebert, L. L. Rutledge, Jr., and A. M. Bernstein, Phys. Rev. C 6, 1254 (1972).

[10]J. C. Hiebert, G. M. Lerner, L. L. Rutledge, Jr., and A. M. Bernstein, Texas A&M University Cyclotron Institute Progress Report, June, 1973 (unpublished).

[11]G. M. Lerner, J. C. Hiebert, L. L. Rutledge, Jr., C. Papanicolas, and A. M. Bernstein, Phys. Rev. C 12, 778 (1975).

[12]A. M. Bernstein and W. A. Seidler, Phys. Lett. 34B, 569 (1971).

[13]A. M. Bernstein and W. A. Seidler, Phys. Lett. 39B, 583 (1972).

[14]W. A. Seidler, Ph.D. dissertation (unpublished).

[15]R. Hofstader, F. Bumiller, and M. R. Yearian, Rev. Mod. Phys. 30, 482 (1958).

[16]B. Tatischeff, I. Brissaud, and L. Bimbot, Phys. Rev. C 5, 234 (1972).

[17]J. A. Nolen, Jr., and J. P. Schiffer, Annu. Rev. Nucl. Sci. 19, 471 (1969).

[18]G. W. Greenlees, V. Hnizdo, O. Karban, J. Lowe, and W. Makofske, Phys. Rev. C 2, 1063 (1970).
[19]R. J. Glauber and G. Matthiae, Nucl. Phys. B21, 135 (1970).
[20]R. A. Schrack, J. L. Leiss, and S. Penner, Phys. Rev. 127, 1772 (1962).
[21]H. Alvensleben, Phys. Rev. Lett. 24, 792 (1970).
[22]E. P. Lippencott and A. M. Bernstein, Phys. Rev. 163, 1170 (1967).
[23]A. Springer and B. G. Harvey, Phys. Lett. 14, 116 (1965).
[24]C. R. Gruhn, T. Y. T. Kuo, C. J. Magiore, H. McManus, F. Petrovich, and B. M. Preedom, Phys. Rev. C 6, 915 (1972).
[25]W. J. Gerace and A. M. Green, Nucl. Phys. A113, 641 (1968).
[26]L. West (unpublished).
[27]G. R. Satchler, Phys. Lett. 39B, 492 (1972).
[28]J. Alster, Phys. Rev. 141, 1138 (1966).
[29]J. Saudinos, G. Vallois, O. Beer, M. Gendrot, and P. Lopato, Phys. Lett. 22, 492 (1966).
[30]M. B. Lewis, F. E. Bertrand, and C. B. Fulmer, Phys. Rev. C 7, 1966 (1973).
[31]F. T. Baker and R. Tickle, Phys. Rev. C 5, 544 (1972).
[32]A. Scott and M. P. Fricke, Phys. Lett. 20, 654 (1966).
[33]R. A. Eisenstein, D. W. Madsen, H. Theissen, L. S. Cardman, and C. K. Bodkelman, Phys. Rev. 188, 1815 (1969).
[34]J. F. Ziegler and G. A. Peterson, Phys. Rev. 165, 1337 (1968).